Highly Efficient Photorefractive Organic Polymers Based on Benzonitrile Shiff Bases Nonlinear Chromophores

ARTICLE *in* THE JOURNAL OF PHYSICAL CHEMISTRY C · NOVEMBER 2011

Impact Factor: 4.77 · DOI: 10.1021/jp206204p

THE JOURNAL OF PHYSICAL CHEMISTRY C

ARTICLE

pubs.acs.org/JPCC

Highly Efficient Photorefractive Organic Polymers Based on Benzonitrile Shiff Bases Nonlinear Chromophores

Victor-Manuel Herrera-Ambriz,[†] José-Luis Maldonado,[†,*] Mario Rodríguez,[†] Rigoberto Castro-Beltrán,[†] Gabriel Ramos-Ortíz,[†] Nancy-Evelyn Magaña-Vergara,[‡] Marco-Antonio Meneses-Nava,[†] Oracio Barbosa-García,[†] Rosa Santillan,[‡] Norberto Farfán,[§] Florian-Xuan Dang,[∥] Pascal G. Lacroix,[∥] and Isabelle Ledoux-Rak[⊥]

[†]Centro de Investigaciones en Óptica, A.P. 1-948, 37000 León, Gto., México

[‡]Departamento de Química, CINVESTAV del IPN, A. P. 14-740, 07000 México D.F., México

[§]Facultad de Química, Departamento de Química Orgánica, UNAM, 04510, México, D.F., México

[∥]Laboratoire de Chimie de Coordination, CNRS, 205 route de Narbonne, 31077 Toulouse, France

[⊥]Laboratorie de Photonique Quantique et Moléculaire, (UMR 8531 du CNRS, Ecole Normale Supérieure de Cachan, Avenue du Président Wilson, 94235, Cachan, France

Supporting Information

ABSTRACT: Photorefractive (PR) materials are ideal for potential applications in real-time optical processing. We report new highly efficient organic photorefractive polymers based on the nonlinear chromophores 4-[(4-(diethylamino)-2-hydroxy-benzylideneamino]benzonitrile (**Dc**) and 4-[4-(diethylamino)-benzylideneamino]benzonitrile (**Ds**). Holographic experiments in a four wave mixing (FWM) and two beam coupling (TBC) geometries were carried out by using a He−Ne laser (633 nm). The electric field steady-state diffraction efficiency dependence was measured. Diffraction efficiency as high as 90% was observed for polymers based on **Dc** at 25 wt % doping level at an external applied electric field around 56 V/μm. For compounds **Dc** and **Ds**, the $\mu\beta$ product was also measured by EFISH technique, **Dc** presents a value 3.5 times higher than **Ds**, which is supported by a theoretical prediction; structural X-ray data and their effect on the PR performance are also discussed. Reversible holographic imaging by using these efficient PR polymers is presented.

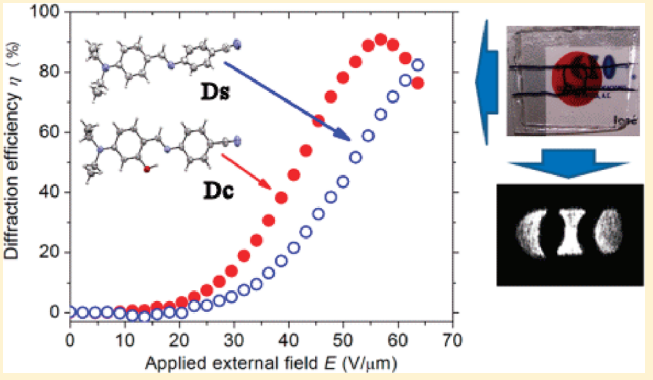

1. INTRODUCTION

A photorefractive (PR) compound needs to simultaneously possess photosensitivity, photoconductivity, and electro-optic (EO) properties. The PR materials are ideal for potential applications in real-time optical processing because they provide a medium for reversible and nonlocal volume holography,[1−6] for instance, very recently the use of PR polymers for demonstration of holographic three-dimensional telepresence was reported.[5] The pioneer report on organic polymer-based PR composites in 1991 by Ducharme et al.,[7] generated intensive research with these materials, and in 1994 appeared the first report of near 100% diffraction efficiency (η) in PR polymers by Meerholz et al.[8] In these PR composites, a spatial optical excitation (interference pattern) produces, through a sensitizer, a number of mobile holes/electrons, which drift under an external applied electric field E, and are subsequently trapped on the dark regions of the interference pattern.[9] The resulting space charge electric field E_{sc}, alters the refractive index of the polymer blend through the electro-optic effect.[9,10] Reorientation of the nonlinear (NL) chromophores under the combined effects of E_{sc} and E, leads to a modulated birefringence, further enhancing the refractive index modulation.[1−4] The resulting index pattern has the same period as the light pattern that generates the photocarriers, but its phase is shifted. This phase shift is an evidence of the PR effect and leads to an energy exchange between the two coherent beams that generate the light grating. For PR polymers, however, a strong external electric field is necessary for charge photogeneration, high hole/electron mobility and orientational birefringence;[11−15] with respect to this fact, in the literature few reports of highly efficient PR polymers at fields lower than 60 V/μm are found,[16−21] so, the reduction of the external applied field value is a feature very

Received: July 1, 2011
Revised: October 11, 2011

   dx.doi.org/10.1021/jp206204p | J. Phys. Chem. C XXXX, XXX, 000–000

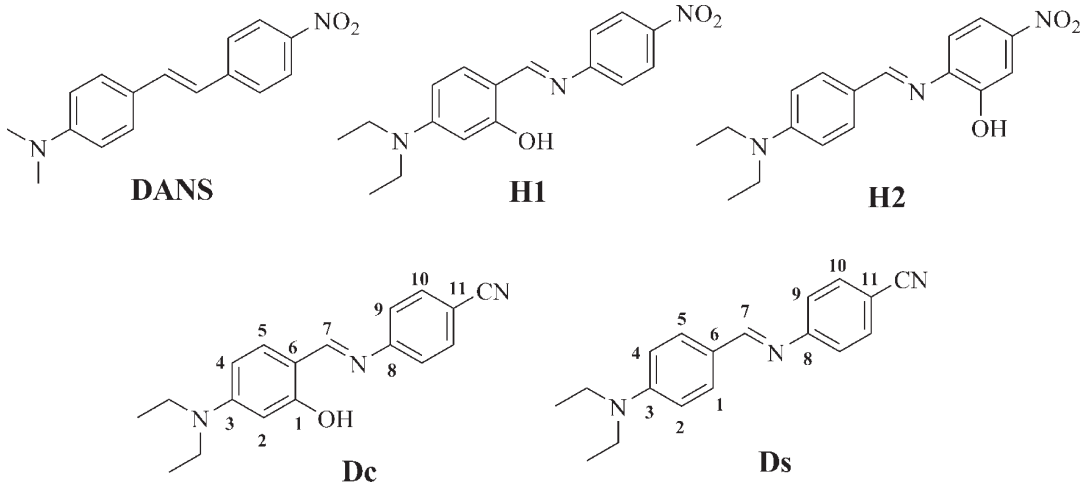

Figure 1. Molecular structure of DANS, H1[32] and H2,[21] and **Dc** and **Ds**.

important to take into account for the scientific research and for technological applications.

Optimization of the PR effect in organic materials, generally involves the synthesis of push-pull molecules (chromophores)[22] with strong linear and microscopic nonlinear optical (NLO) properties, i.e., the permanent dipole moment μ, the polarizability anisotropy $\Delta\alpha$ (birefringence contribution), and the first hyperpolarizability β (EO contribution).[23,24] For polymers with glass transition temperature (T_g) near to the working temperature (T),[25,26] a possible figure of merit (FOM) to estimate the efficiency of the chromophores has been defined as follows:[23]

$$\mathrm{FOM} = 2/(9K_BT)\Delta\alpha\mu^2 + \beta\mu \quad (1)$$

Among the most successful NLO chromophores used in PR polymer composites are[3,12] azo dyes (i.e., DMNPAA), oxopyridone derivatives (i.e., ATOP-3), dicyanostyrene derivatives (i.e., AODCST), dicyanomethylenedihydrofuran derivatives (i.e., DCDHF-6), pyridone derivatives (i.e., 2BNCM), rigid polyene derivatives (i.e., DHADC-MPN), etc. However, the 4-dimethylamino-4-nitrostilbene (DANS,[2,27] see Figure 1) was used as a typical NLO molecule during the 1980s. Among the stilbene derivatives with different terminal groups, DANS presents some of the largest NLO properties, i.e., $\mu = 6.6$ D, $\beta = 73 \times 10^{-30}$ esu and $\gamma = 225 \times 10^{-36}$ esu.[27] The influence of substitution, conjugation length, and planarity (besides excellent solubility in organic solvents) of the molecules on their NLO properties[2] are all very important aspects to be considered when searching for optimized structures for efficient electro-optic and NLO effects in general. Recently, we reported very good results on the diffraction efficiency at low applied electric field on PR compounds based on the arylimine chromophores H1 and H2,[21] see Figure 1, obtaining 87% at $E = 48$ V/μm and 75% at just $E = 32$ V/μm, respectively.

In ref 28, some numerical values for the FOM given by eq 1 are summarized (in ref 28, this FOM was defined dividing eq 1 by M/9 with M the molar mass, see also ref 12), for instance: for the azo dye DMNPAA, FOM = 0.2 and for the chromophore DHADC-MPN, FOM = 0.6, the units are 10^{-74} $V^{-2}C^2m^4kg^{-1}$ mol. DHADC-MPN had a better PR performance than DMNPAA[8,16,29] even when the DHADC-MPN concentration was of 40 and 25 wt % and the doping level DMNPAA was of 50 wt %.

However, considering the overall PR performance,[30] various additional properties of the NLO chromophores need to be taken into account. For example, a high concentration of the chromophores is desirable to maximize electric field-induced birefringence, however, the addition of high concentrations of small molecules (highly dipolar chromophores) can cause PR composites to undergo phase separation, which affects their optical transparency and reduces the shelf-life time. The high concentration of highly polar chromophores that possess large FOMs may also reduce the charge carrier mobility[12,13,28] in the composites. Furthermore, there is spectroscopic evidence of dimer and aggregate formation in PR composites with high chromophore content,[12] which may influence the electro-optic response. Finally, the HOMO energy levels of the transport molecules and the electro-optic chromophores play an important role in the buildup of radical ions of the sensitizer, for instance, in PVK-based materials sensitized with C_{60} and doped with low-ionization potential chromophores, continuous exposure will lead to an accumulation of C_{60} radical anions (deep traps), which gradually decreases the photoconductivity[3] and slows down the response time. This deterioration of the response time can be minimized by using chromophores with higher ionization potential; however, such compounds often lead to lower dynamic range. Thus, the ability to control the relative energy levels of the frontier orbitals of the different molecules doped into these photorefractive polymers will play an important role in making materials that are stable under continuous operation.[3]

Here we report on the sample fabrication, diffraction efficiency, refractive index modulation, optical gain, and dynamic holographic imaging of PR polymers based on **Dc** and **Ds** (see Figure 1). The compounds **Dc** and **Ds** contain the CN acceptor group on the main π-backbone instead of the NO_2 fragment as in H1 and H2; they also have an excellent optical transparency in the visible region. These compounds were synthesized in order to evaluate the effect of the acceptor moiety on the reorientation process of the chromophore molecules and on the diffraction efficiency, in PR composites, as well as to correlate their $\mu\beta$ values with experimental PR results. Experimental and computational estimations for the $\mu\beta$ product through the electric field induced second harmonic (EFISH) technique and ZINDO data,[31] respectively, are investigated. Torsion angles between the two phenyl rings of **Dc** and **Ds** and their PR effect are also

dx.doi.org/10.1021/jp206204p |J. Phys. Chem. C XXXX, XXX, 000–000

compared and discussed through X-ray data. Finally, holographic recording imaging is demonstrated at relatively low electric field (20 V/μm) with respect to that reported in the literature for other PR polymers.

2. EXPERIMENTAL SECTION

2.1. Materials. **Dc** and **Ds** were synthesized in our laboratories according to the typical synthesis procedure[33] by condensation reaction between 4-aminobenzonitrile and 4-diethylaminosalicilaldehyde for **Dc** and with 4-diethylaminobenzaldehyde for **Ds**. Starting materials and solvents were purchased from Sigma-Aldrich distributor and all of them were used without further purification. Melting points were obtained with an Electrothermal 9200 apparatus and are uncorrected. Infrared spectra were measured on an FTIR Varian Spectrophotometer ATR. ^{1}H and ^{13}C spectra as well as homo and hetero correlation spectroscopy (^{1}H−^{1}H COSY and ^{1}H−^{13}C HETCOR) were recorded on JEOL eclipse ECA +500 spectrophotometer. Chemical shifts (ppm) are relative to $(CH_3)_4Si$ for ^{1}H and ^{13}C.

2.1.1. ***Dc*** *(E)-4-(4-(Diethylamino)-2-hydroxybenzylideneamino)benzonitrile.* M.P.: 148.3−149.6 °C. IR(KBr)ν_{max}: 3439, 2978, 2938, 2220, 1629, 1590, 1518, 1427, 1340, 1246, 1168, 1136, 985, 817 cm^{-1}. ^{1}H NMR ($CDCl_3$, 500 MHz) δ: 8.38 (1H, s, H-7), 7.62 (2H, d, J = 8.7 Hz, H-10), 7.22 (2H, d, J = 8.7 Hz, H-9), 7.15 (1H, d, J = 8.8 Hz, H-5), 6.25 (1H, dd, J = 8.8, 2.4 Hz, H-4), 6.16 (1H, d, J = 2.4 Hz, H-2), 3.39 (4H, q, J = 6.9 Hz, N−CH_2), 1.20 (6H, t, J = 6.9 Hz, −CH_3) ppm. ^{13}C NMR ($CDCl_3$, 125 MHz) δ: 164.2 (C-1), 162.2 (C-7), 153.1 (C-8), 152.6 (C-3), 134.5 (C-5), 133.4 (C-10), 121.7 (C-9), 119.2 (CN), 109.0 (C-11), 108.2 (C-6), 104.4 (C-4), 97.6 (C-2), 44.7 (N−CH_2), 12.7 (−CH_3) ppm. HR-APCI-MS: for $C_{18}H_{20}N_3O$ $[M^+ + H]^+$: 294.1606; found: 294.1600 error 0.3021 ppm.

2.1.2. ***Ds*** *(E)-4-(4-(Diethylamino)benzylideneamino)benzonitrile.* M.P.: 143.2−144.3 °C. IR (KBr)ν_{max}: 2971, 2893, 2218, 1575, 1546, 1524, 1405, 1267, 1117, 1151, 985, 842, 818 cm^{-1}. ^{1}H NMR ($CDCl_3$, 500 MHz) δ: 8.22 (1H, s, H-7), 7.72 (2H, d, J = 9.0 Hz, H-1,5) 7.61 (2H, d, J = 8.6 Hz, H-10), 7.18 (2H, d, J = 8.6 Hz, H-9), 6.70 (2H, d, J = 9.0 Hz, H-2,4), 3.42 (4H, q, J = 6.9 Hz, N−CH_2), 1.20 (6H, t, J = 6.9 Hz, −CH_3) ppm. ^{13}C NMR ($CDCl_3$, 125 MHz) δ: 161.8 (C-7), 157.2 (C-8), 150.8 (C-3), 133.3 (C-10), 131.4 (C-1,5), 122.9 (C-6), 121.8 (C-9), 119.5 (CN), 111.1 (C-2,4), 107.7 (C-11), 44.6 (N−CH_2), 12.6 (−CH_3) ppm. HR-APCI-MS: for $C_{18}H_{20}N_3$ $[M^+ + H]^+$: 278.1657; found: 278.1601 error: 0.3018:

2.2. X-ray Measurements. The single crystals of **Dc** and **Ds** suitable for X-ray structural studies were obtained by slow solvent evaporation at room temperature from saturated solutions of $CHCl_3$ or CH_2Cl_2. The crystal data were measured using an Enraf Nonius Kappa-CCD with graphite-monochromated $\lambda_{Mo\ K\alpha}$= 0.710 73 Å. Frames were collected at T = 293 K via ω/φ rotation. All reflection data set were corrected for Lorentz and polarization effects. The first structure solution was obtained using the SHELXS- 97 and SIR2004 programs and then the SHELXL-97 program for refinement and output data was applied. All heavier atoms were found by Fourier map difference and refined anisotropically. C−H hydrogen atoms were placed in a geometrically calculated position using a riding model. O−H hydrogen atom has been localized by difference Fourier maps and its bond distance and isotropic temperature factor have been refined freely. All software manipulations were done under the WinGX environment program set.[34] Molecular perspectives were drawn under Mercury drawing application.

2.3. EFISH Experiments. The first hyperpolarizability (β) was experimentally determined using the electric field induced second-harmonic (EFISH) technique as a $\mu\beta$ product.[35] Briefly, the EFISH experimental method is described as follows: an Nd:YAG laser emitting picosecond pulses (1.064 μm at 10 Hz repetition rate) was used to pump a hydrogen cell (1 m long, 50 bar). The outcoming Stokes-shifted radiation at 1.907 μm generated by the Raman effect was used as the fundamental beam for carrying out the EFISH experiments. This fundamental beam was focused into a solution of **Dc** and **Ds** in dichloromethane (at concentrations of 5 mM and 10 mM), contained in a quartz cell with windows in a wedge configuration in order to generate the Maker fringe pattern as a function of the cell translation. The centrosymmetry of the solution was broken by dipolar orientation of the chromophores when a high voltage signal (5 kV) synchronized with the laser pulse was applied to the solution. The generated second-harmonic signal (at 953.5 nm) was selected through a suitable interference filter, and detected by a photomultiplier tube.

2.4. Theoretical Methods. The electronic spectra of **Dc** and **Ds** were computed using the *Materials Studio* program package.[36] The metric parameters used for the calculations were taken from the present X-ray diffraction data. The Zerner's intermediate neglect differential overlap (ZINDO)[37] method was employed for the calculation of the spectra with the INDO/1 Hamiltonian. The 100 simple excitations between the 10 highest occupied orbitals and the 10 lowest unoccupied ones were allowed to mix in the configuration interaction (CIS) process.

2.5. PR Sample Preparation. We made thick, solid film samples of **Dc** and **Ds** in combination with the widely used mixture of PVK:ECZ:C_{60}, PVK being the photoconducting polymer matrix and ECZ the plasticizer,[1−4,6,12,38] at 25:49:25:1 wt %. Magnetic stirring in dichloromethane dissolved the **Dc** or **Ds**:PVK:ECZ constituents. The sensitizer fullerene C_{60} was previously dissolved in toluene and then mixed with the **Dc** or **Ds**:PVK:ECZ solution. The final mix was filtered through an 11 μm pore size paper filter. The solvent was evaporated under reduced pressure on a rotary evaporator, and the mixture was subsequently dried in an oven at 60 °C, for 12 h. Next, the dried material was melted and mixed within two large glass slides. A small piece of the resulting film was cut and melted between two ITO-coated glass slides at a temperature of about 145−160 °C. Calibrated glass spacers of thickness d = 110 μm were used to ensure a uniform sample thickness.

2.6. Holographic Experiments. The performance of our PR polymers was tested with a tilted four wave mixing (FWM) and two beam coupling (TBC) geometries,[11] details of our experimental setup can be found elsewhere.[21,39] Figure 2a shows the used geometry. Briefly, our experiments were performed with a 10 mW He−Ne laser (λ = 633 nm). The writing beams (WBs) had s-polarization, with power of ∼0.7 mW each. They were focused on the sample, with a spot size of ∼500 μm at their focal planes, so, the recording light intensities (I) were of ∼350 mW/cm^2. The angle $2\theta_o$ ($\alpha_2 - \alpha_1$) between the writing beams outside the sample was 21°, whereas the tilt angle ψ was 60°. The refractive index of the polymer composites, measured with a reflectometer (Filmetrics F20), resulted in n = 1.58−1.60 at 633 nm. The grating spacing under these conditions was 2.9 μm.[11,21,39] The measurements of the diffraction efficiency were carried out with a p-polarized probe/reading beam with a power

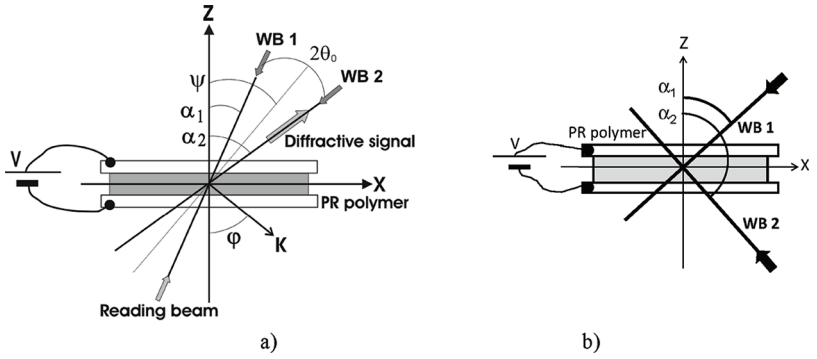

Figure 2. (a) Transmission geometry mainly used in the four and two beam coupling (FWM and TBC) measurements and holographic imaging: WB = writing beam, ψ = tilt angle, $2\theta_o = (\alpha_2 - \alpha_1)$ = angle between the WBs, φ = angle of the grating vector. In the TBC geometry, the reading beam is blocked. (b) Reflection geometry for TBC.

of only a thousandth (1/1000) of the power of the writing beams. An FWM geometry typically has a different polarization for the writing beams and reading beam in order to neglect possible effects of the probe beam on the grating even when its intensity is much weaker than that of the writing beams.

Although other poling configurations exist, such as the reflection geometry,[40−43] most of the diffraction experiments have been performed so far in the tilted geometry. In reflection geometry (see Figure 2b), for the short grating spacings obtained (~0.2 μm), very large space-charge modulation amplitude is required to sustain significant space-charge fields. Most conventional photorefractive polymers fail in this respect. The resulting gain coefficients and refractive index changes in reflection geometry tend, therefore, to be rather small. For this reason, until now, only a few reports have discussed this configuration for photorefractive polymers,[40−43] however, in ref 42, high performance reflection gratings are noted.

As a demonstration for holographic application, we recorded holograms of two-dimensional objects (of about 5 mm in size) on a slide. In dynamic holography, a hologram can be stored, or erased, without the need of a development step. It can be used in an unlimited number of write-erase cycles, and can virtually display information in real time. In our case, holographic images were acquired by using the Bragg diffraction of a reading beam (diffracted phase conjugated signal). To have control over the beam size (about 8 mm in diameter) a beam expander (Galilean telescope) was implemented. In the formation of dynamic holographic images, the probe beam was *p*-polarized, and was sent into the PR polymer with a spot size of ~2 mm in the vicinity of the sample. After reconstruction, the holographic images were sent into a small, simple, and inexpensive CCD camera eliminating with this the need for electronic processing.

3. RESULTS AND DISCUSSION

3.1. Structural Studies. Schiff bases **Dc** and **Ds** are yellow solids soluble in common organic solvents; as first approximation ^{1}H and ^{13}C NMR experiments were employed to establish the imine bond formation and the "push-pull" stilbazole-like structure on **Dc** and **Ds**. Furthermore, X-ray diffraction analysis (see Table 1) for crystals **Dc** and **Ds** were used to corroborate their configuration, both compounds crystallize on triclinic space group $P\bar{1}$ containing two molecules per unit cell (Figure 3). In general, the X-ray data for **Dc** and **Ds** imines show a linear π-backbone with dipolar architecture due to the donor (Et_2N-) and the acceptor (−CN) groups, for **Dc** a phenol moiety complete the structure. Detailed analyses indicate that the **Dc** compound shows a near planar conformation for the complete π-backbone system, which could be promoted by the intramolecular hydrogen bond (N···H−O), the phenyl rings contained in the structure are deviated 2.7° out of the planarity (with respect to the main π-system). In contrast, **Ds** imine does not show any intramolecular hydrogen bond, as a consequence the phenyl fragments have a deviation of 50° with respect to the π-backbone plane, and the conformation is non planar.

Analysis of the intramolecular hydrogen bond parameters in **Dc** shows an O···N distance of 2.5909(19) Å, which is less than 3.07 Å (sum of its van der Waals radii) and an O−H···N angle of 149(3)°. This hydrogen bond could promote a possible tautomeric equilibrium between the enol and keto forms on orto-hydroxy Shiff bases,[44] as could be the case in this **Dc** compound. In this sense, the distance of C−O bond (1.3487(18) Å)

Table 1. Summarized Data for Crystals of Dc and Ds

crystal data[a]	Dc	Ds
formula	$C_{18}H_{19}N_3O$	$C_{18}H_{19}N_3$
MW (g/mol)	293.36	277.36
crystal system	triclinic	triclinic
space group	$P\bar{1}$	$P\bar{1}$
a (Å)	6.5560(2)	7.6934(2)
b (Å)	7.6970(2)	9.7091(3)
c (Å)	17.4380(10)	11.3685(3)
α (°)	93.7540(10)	84.576(1)
β (°)	97.2560(10)	73.338(2)
γ (°)	116.53(2)	75.881(1)
V (Å^3)	773.58(5)	788.68(4)
Z	2	2
ρ_{calc} (g/cm^3)	1.259	1.168
collected refl.	8703	12077
ind. refl.	3402	3545
observed refl.	2117	2182
R $[I > 2\sigma(I)]^b$	0.068	0.056
R_w (all data)[c]	0.1178	0.173
$\Delta\rho_{max}$ (e Å^{-3})	0.19	0.18
$\Delta\rho_{min}$ (e Å^{-3})	−0.18	−0.21

[a] $\lambda_{MoK\alpha}$ = 0.7103 Å. [b] $R = \Sigma(F_o^2 - F_c^2)/\Sigma F_o^2$. [c] $R_w = [\Sigma w(F_o^2 - F_c^2)^2/\Sigma w(F_o^2)^2]$.

dx.doi.org/10.1021/jp206204p |J. Phys. Chem. C XXXX, XXX, 000–000

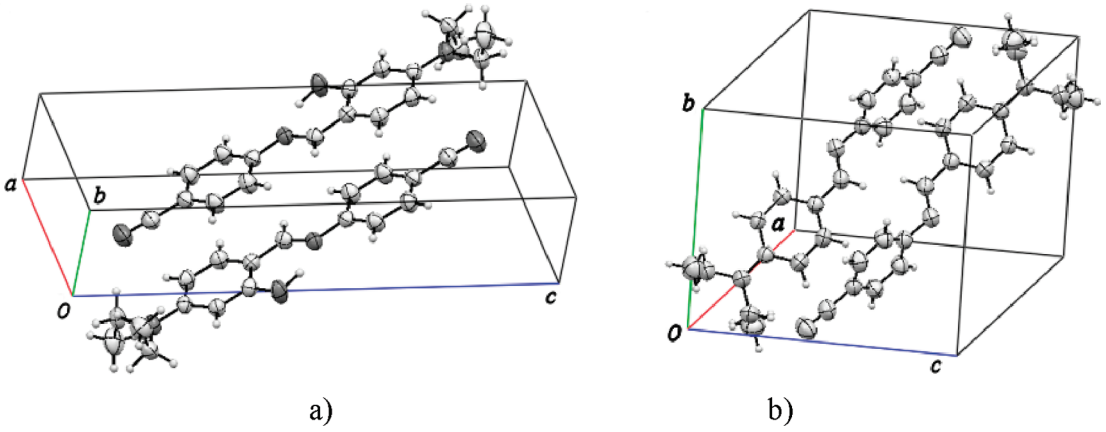

Figure 3. Crystal packing of imines **Dc** (a) and **Ds** (b) ellipsoids are drawn at 50% of probability.

Table 2. Oxidation Onset Potential and Estimated E_{HOMO} of the NL Chromophores Described in This Study

chromophore	E_{pa} vs SCE[a] (V)	oxidation onset potential vs SCE (V)	$-IP\ (E_{HOMO}) = -E^{Ox}_{onset}$(vs SCE) + 4.39 (eV)
Dc	1.066	0.947	−5.34
Ds	1.120[b]	0.987	−5.38

[a] Electrochemical experiments were carried out using an $Ag/AgNO_3$ (0.1M) reference electrode with E = 0.3 V vs SCE. [b] **Ds** showed a fast reversible system E_{pc} = 1.05 V with ΔE_p= 0.07 V.

indicates certain Keto character present on **Dc** when is compared to the standard C−O bond length of 1.43 Å. The imine bond in **Ds** has a length of 1.279(2) Å, which is shorter than that for **Dc**: 1.296(2) Å; the opposite tendency is observed for the C_{ph}−C distance: A larger length value is detected in **Ds** (1.448(2)Å) than in **Dc** (1.421(3)Å). So, it is highly probable to have a Keto character on the imine **Dc** and this fact also could be related with its planar conformation.[45]

3.2. Cyclic Voltammetry Measurements and E_{HOMO} Values. The HOMO energy levels for **Dc** and **Ds** chromophores, that are correlated with their ionization potential IP, were estimated (see Table 2) from cyclic voltammograms measuring the electrochemical onset oxidation potential (vs SCE reference electrode) as previously described.[46] These chromophores did not show reduction signals in the electrochemical system used for the analysis (CH_2Cl_2 tetrabutylammonium perchlorate 0.1M), therefore the electron affinities EA and LUMO energies values could not be determined.

3.3. Molecular Linear and Nonlinear Optical Properties. Figure 4 shows the linear optical absorption of the prepared PR composites films, and the UV−vis spectra of **Dc** and **Ds** are shown in the inset. Both chromophores exhibit an intense and low lying band with absorption maxima (λ_{max}) centered at 401 and 382 nm, for **Dc** and **Ds**, respectively. The experimental and ZINDO computed data are compared in Table 3. Although the computed data are blue-shifted with respect to the experimental ones, the agreement is satisfactory and suggests that the computation can successfully be used for qualitatively describing the origin of the difference in the NLO response of **Dc** and **Ds**.

It has long been established that pseudolinear "push-pull" stilbazole-like chromophores possess NLO responses, which are

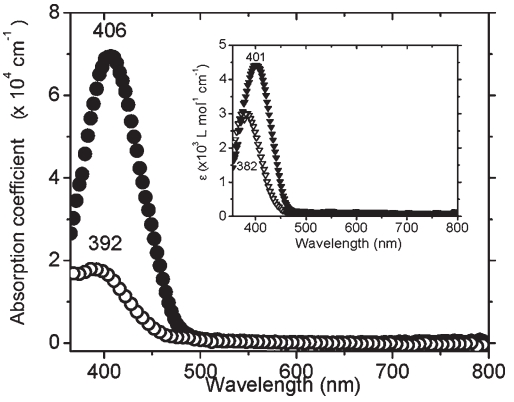

Figure 4. Absorption coefficient of **Dc**:PVK:ECZ:C_{60} (filled circles) and **Ds**:PVK:ECZ:C_{60} (open circles) at 25:49:25:1 wt %. Inset: absorption of **Dc** (filled triangles) and **Ds** (open triangles) in solution (chloroform).

strongly correlated with an intense and low-lying HOMO → LUMO (HL)-based transitions having strong charge transfer character.[47] A simplified but widely used two level description has been employed to quantify the molecular hyperpolarizability (β) as follows:[48,49]

$$\beta = \frac{3e^2\hbar f \Delta\mu}{2mE_{HL}^3} \times \frac{E_{HL}^4}{(E_{HL}^2 - (2\hbar\omega)^2)(E_{HL}^2 - (\hbar\omega)^2)} \qquad (2)$$

In this equation, f, $\Delta\mu$, and E_{HL} are the oscillator strength, the difference between ground and excited state dipole moment, and the energy of the HOMO → LUMO based transition, respectively ($\hbar\omega$ being the energy of the incident laser beam). The computed data are gathered in Table 4 and compared with the EFISH data available. The differences observed in E_{HL}, f, and mainly in the charge transfer ($\Delta\mu$) lead to a NLO response ($\beta\mu$) increased by a factor 3.8, on passing from **Ds** to **Dc**, which is in good agreement with the factor 3.5 determined by EFISH experiments. Although experiment and theory show a significant discrepancy in the magnitude of $\beta\mu$, the computation qualitatively accounts for the differences observed in the NLO properties of the two molecules under investigation.

3.4. Photorefractive Properties. Figure 5 shows the normalized (internal) diffraction efficiency, obtained from FWM experiments, as a function of the external applied electric field (E)

dx.doi.org/10.1021/jp206204p |J. Phys. Chem. C XXXX, XXX, 000–000

Table 3. Experimental Spectroscopic (λ_{max} in nm, Extinction Coefficients (ε) in L mol^{-1} cm^{-1}) and ZINDO Computed Data (Oscillator Strength (f)), and CIS Expansion for the Dominant Transition of Dc and Ds

	experimental data		computed data		
	λ_{max}	ε	λ_{max}	f	composition of CIS expansion[a]
Dc	401	4420	358	1.25	$-0.939\ \chi_{56\rightarrow57}$
Ds	382	3020	325	1.03	$-0.822\ \chi_{53\rightarrow54} + 0.333\ \chi_{52\rightarrow54}$

[a] Orbital 56 is the HOMO and orbital 57 the LUMO for **Dc**. Orbital 53 is the HOMO and orbital 54 the LUMO for **Ds**.

Table 4. Computed (in nm, $\Delta\mu$ in D, β in 10^{-30} esu, μ in D) and Experimental EFISH Data for Dc and Ds, at 1.907 μm

	computation (ZINDO)						experiment (EFISH)
	λ_{max}	f	$\Delta\mu$	β	μ	$\beta\mu$[a]	$\beta\mu$[b]
Dc	358	1.25	4.2	15.8	9.08	143.5	320
Ds	325	1.03	1.8	4.02	9.38	37.7	90

[a] It is assumed that β and μ are parallel, which is a common approximation in "push-pull" chromophores. [b] For DANS $\mu\beta = 482 \times 10^{-30}$ esu·D[27] and for H1 $\mu\beta = 422 \times 10^{-30}$ esu·D. For DHADC-MPN: $\mu\beta = 756 \times 10^{-30}$ esu·D,[16] DMNPAA: $\mu\beta = 264 \times 10^{-30}$ esu·D[16]. NPADVBB: $\mu\beta = 192 \times 10^{-30}$ esu·D.[16,50]

for samples with composition **Dc** or **Ds**:PVK:ECZ:C_{60} at 25:49:25:1 wt %. To obtain a stable value for each datum, it took 7 min to collect the 60 data points (computer data acquisition) in the plot. The diffraction efficiency η is defined in eq 3 where I_{diffr} is the intensity of the diffracted beam and I_{trans} is the intensity of the transmitted probe beam through the film.

$$\eta = \frac{I_{diffr}}{I_{diffr} + I_{trans}} \tag{3}$$

PR compounds based on **Dc** showed a maximum diffraction efficiency of 90% at 56 V/μm and for those based on **Ds**, 82% at 63 V/μm. For PR polymers based on **Dc**, overmodulation, i.e., diffraction efficiency curve with a maximum peak,[16,19,20,50] was observed. This overmodulation can be explained in terms of eq 4, it is briefly mentioned in the two sentences below this equation. We can see that **Dc** compound containing the OH group bonded to the diethylaminophenyl ring gave a slightly higher η value than that of PR polymers based on **Ds**, one of the reasons is probably due to a larger planarity of the π-backbone in **Dc** as can be depicted from the X-ray analysis: The torsion angles between the two phenyl rings in **Dc** and **Ds** were 2.7° and 50° (X-ray data), respectively. Molecular planarity promotes π-conjugation, which is desirable to attain high nonlinearities. Indeed, ONL measurements by EFISH technique showed that **Dc** compound has a $\mu\beta$ value equal to 320×10^{-30} esu·D, which is about three and a half times larger than that measured for **Ds**: 90×10^{-30} esu·D; this is an important feature that could partially explain the better PR response on those polymers based on **Dc** since its larger value for the product $\mu\beta$ might favor a better directional dipolar orientation upon the applied external electric field, which in turn also implies a larger electro-optical tensor element for the corresponding comosite.

Different sensitizers are used for PR materials, for instance, fullerenes and inorganic nanoparticles such as CdS, CdTe, and CdSe,[6,12,38,51,52] however, fullerene C_{60} is still one of the best

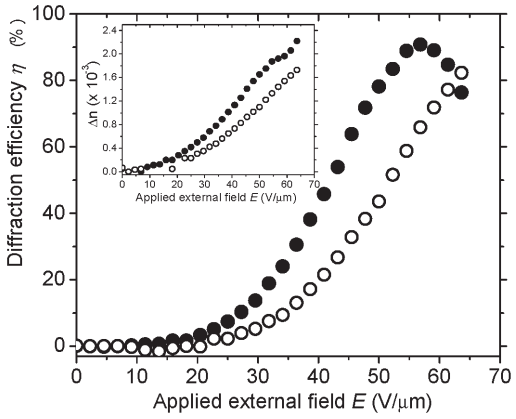

Figure 5. Normalized η as a function of E for the PR polymers **Dc**:PVK:ECZ:C_{60} (filled circles), **Ds**:PVK:ECZ:C_{60} (open circles) at 25:49:25:1 wt %. Inset: corresponding refractive index modulation Δn for **Dc**:PVK:ECZ:C_{60} (filled circles) and **Ds**:PVK:ECZ:C_{60} (open circles).

molecules for this purpose,[6] for instance, in ref 52, for PR polymers sensitized with CdTe and CdSe nanoparticles a diffraction efficiency of less than 16% is obtained at E = 60 V/μm and in ref 51., PR polymers sensitized with CdS nanoparticles a diffraction efficiency of just 4.4% is measured but a zero electric field. In comparison with some highly efficient PR polymers that have been reported using different chromophores (or mixtures), photoconductors, plasticizers, and sensitizers at different doping levels, our PR samples showed quite encouraging results in terms of diffraction efficiency at moderated external applied electric fields (<60 V/μm),[6] with just 25 wt % of chromophore amount, which is one of the lowest chromophore concentrations reported.[12,16−20] In Table 4 summarized the holographic values of some of the best-performing PR polymer composites reported in the literature for the visible red wavelength region. For instance, only polymer composites 2 by Hendrickx et al.,[17] and 3 by Joo et al.,[18] gave high diffraction efficiencies at a relatively very low applied field of 28 and 30 V/μm, respectively, but with higher chromophore content (37.6 and 30 wt.%, respectively) than our PR polymers based on **Dc** and **Ds**. Also, in our previous work,[21] a 75% diffraction efficiency was measured at just 32 V/μm for PR polymers based on H2 (see Figure 1). It should be recalled that diffraction efficiency increases as the fourth power of the applied field.[53] The inset in Figure 5 shows the values for the refractive index modulation Δn, corresponding to η measured for **Dc**- and **Ds**-based polymers. These values were calculated from eq 4 that provide a relation between η and Δn (Kogelnik's theory):[23,50,54]

$$\eta(\Delta n) \approx \sin^2\left(\frac{\pi \Delta n(E) d}{\lambda \cos\ \psi_{int}}\right) \tag{4}$$

where ψ_{int} is the tilt angle inside the sample. In eq 4, Δn is continuously increasing as a function of the applied field but η is not (see Figure 5). We found a large dynamic range for **Dc**-based polymers: $\Delta n = 2.22 \times 10^{-3}$ at 64 V/μm and for **Ds** based compounds: $\Delta n = 1.73 \times 10^{-3}$ at the same applied external field. Table 4 also includes some measures from the literature for the refractive index modulation, we can see that our Δn values are very acceptable.

The primary role of a sensitizer added to the PR material is to assist in charge photogeneration. The choice of a sensitizer

dx.doi.org/10.1021/jp206204p | J. Phys. Chem. C XXXX, XXX, 000–000

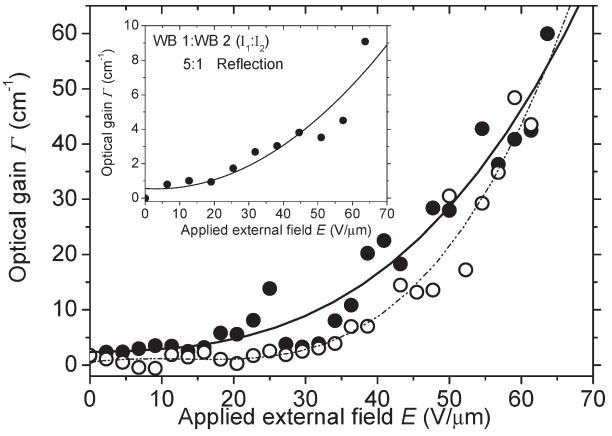

Figure 6. Gain coefficient Γ as a function of the applied electric field E for the composites **Dc**:PVK:ECZ:C_{60} (filled circles) and **Ds**:PVK:ECZ:C_{60} (open circles) at 25:49:25:1 wt % for transmission geometry. Inset: Gain coefficient for reflection geometry, beam ratio (I_1:I_2) 5:1.

depends on the desired wavelength sensitivity and is often dictated by the transport molecule and in some cases, by the chromophores as well. The best performance is obtained by optimizing the charge-transfer (CT) properties between a given sensitizer and its parent transport molecule. The most successful class of sensitizers to date remains the CT complexes formed between a donor-like and an acceptor-like molecule or moiety, as in the case of PVK:C_{60}. The intermolecular interaction (partial charge transfer) between the donor D and the acceptor A molecules leads to a new absorption band that does not appear in the spectrum of either component alone. In our case, it is also possible that there exist a charge-transfer complex between C_{60} and **Dc**,**Ds** in order to have a weak (but enough) absorption, specifically at 633 nm. Moreover, the sensitizer is a major player in the steady-state properties of a PR material as it is also linked to charge trapping, one of the crucial processes in PR grating formation.[12]

The traps present in the material limit the migration process which can take place on micrometer length scales. Charges trapped in dark regions of the interference pattern and those opposite charges left behind in illuminated regions give rise to an inhomogeneous space charge distribution that leads to the necessary space charge electric field for the PR phenomenon. In our case, the highest occupied molecular orbital (HOMO) energy level of PVK is −5.92 eV, when the sensitizer (C_{60}) is irradiated, electrons are excited from its HOMO energy level (−6.4 eV) to its LUMO level. The holes thus generated are transferred to the donor molecules (PVK in this case). These holes hop through the donor molecules until they get trapped. In the case of the PVK system, the chromophores could act as traps since, usually; their energy levels are above PVK's.[4,12] Furthermore, the accumulation of deep traps as the material is continuously light exposed takes place here. By cyclic voltammetry measurements,[46] the HOMO levels of chromophores **Dc** and **Ds** were (see Table 2) −5.34 and −5.38 eV, respectively.

Figure 6 shows the TBC performance as a proof of the PR nature. These TBC experiments, in transmission geometry, were performed under the same angle parameters than FWM (see Figure 2a) and with the same experimental setup by just blocking the reading beam. In this case, the writing beams were p-polarized with an intensity ratio of 4:1 (I_1:I_2). A general expression for the optical gain coefficient Γ, for transmission geometry, can be obtained from Kukhtarev's theory of dynamic self-diffraction in a photorefractive medium:[6,11,29,50]

$$\Gamma(\Delta n,\phi) = \frac{4\pi}{\lambda}(\hat{e}_1\cdot\hat{e}^*_2)\Delta n\sin\phi = \frac{1}{d}\left[\cos\alpha_{1\text{int}}\ln\left(\frac{I^t_1(I_2\neq 0)}{I^t_1(I_2=0)}\right) - \cos\alpha_{2\text{int}}\ln\left(\frac{I^t_2(I_1\neq 0)}{I^t_2(I_1=0)}\right)\right] \quad (5)$$

where $\hat{e}_i$ are the polarization vectors of the incoming beams, ϕ is the phase shift between the intensity and the Δn patterns, I^t_1 and I^t_2 are the transmitted intensities of the two writing beams, and $\alpha_{1\text{int}}$ and $\alpha_{2\text{int}}$ are the writing beams angles inside the sample. The maximum gain coefficient Γ, estimated from eq 5, for **Dc**:PVK:ECZ:C_{60} was about 60 cm^{-1} at E = 63 V/μm and for **Ds**:PVK:ECZ:C_{60} about 48 cm^{-1} at E = 59 V/μm. From the absorption coefficient α, for polymers based on **Dc** (∼35 cm^{-1} at 633 nm) and on **Ds** (∼30 cm^{-1} at 633 nm), it can be observed that a net optical gain ($\Gamma_n = \Gamma - \alpha$) was obtained: 25 and 18 cm^{-1}, respectively. In this case, and according to the data in Table 5, the gain coefficient Γ is not optimized for these PR devices based on the chromophores **Dc** and **Ds**. Table 6 summarizes all the holographic experimental results for our PR polymers.

However, the tilt of the recording beams, in transmission geometry, with respect to the sample normal assures that the large electric field being applied across the relatively thin sample has a significant projection along the grating vector. This dramatically enhances the charge separation and the resulting space-charge field E_{sc}. An even better projection would be achieved if the grating vector also lies normal to the sample, as it is in the case of reflection geometry where beams arrive from opposite surfaces. However, as was mentioned in Section 2.6, for the short grating spacings (∼0.2 μm) obtained with such geometry (see Figure 2b), a large space-charge modulation amplitude is required to sustain significant space-charge fields; it is explained by an increase of the trapping sites density N_{eff}, with the applied external field, which give rise to an increase of the saturation field E_q and consequently an increased space charge field E_{sc}.[40−42] Physically, this is related to the field dependence of the charge-carrier generation efficiency and, therefore, to a field-enhanced (quasi-steady-state) density of ionized sensitizer units, and as was explained; they can act as deep traps. Furthermore, the density of trapping sites can be improved by selecting composite elements with appropriate energy levels to trap holes.[4] Additionally, due to the reduced grating spacing, the recording speed in the reflection geometry is usually faster than in transmission geometry under similar experimental conditions. Here, we also performed TBC experiments in this reflection geometry for our PR samples, data are shown in the inset of Figure 6 by using $\alpha_1 = 30°$ and $\alpha_2 = 135°$ and following the procedures described in ref 42 obtaining small values (∼9 cm^{-1} at 63 V/μm, for PR polymers based on **Dc**) in comparison, for instance, to those obtained in refs 40 and 42 of 104 and 260 cm^{-1} at 60 V/μm, respectively. In ref 42, they estimated an N_{eff} of about 7×10^{16} cm^{-3}.

As a demonstration for holographic application, Figure 7a shows a photograph of the image of an object (logo of CIO institution) and Figure 7b shows the corresponding photograph of the holographic image. The resolution of the holographic system was limited by the CCD pixel size. Images were formed in less than ∼0.5 s, which is a reasonably short period of time.[52]

dx.doi.org/10.1021/jp206204p |J. Phys. Chem. C XXXX, XXX, 000–000

Table 5. Holographic Parameters for Some Highly Efficient PR Polymers That Have Been Reported at External Electric Fields Lower than 60 V/μm (Except for Γ in Some Cases) in the Visible Part of the Spectrum[a]

	polymer composite (weight % ratios)	λ, nm	Δn, $\times 10^{-3}$ (E, V/μm)	Γ, cm^{-1} (E, V/μm)	η_{max}, % (E, V/μm)	ref.
1	DHADC-MPN:PVK:ECZ:TNF (40:39:19:2)	633	4.4 (40)		10^{ext} (30)	16
2	DHADC-MPN:PTCB:DIP:TNFDM (37.6:49.7:12.5:0.18)	633	8.5 (50)	225 (50)	71^{ext} (28)	17
3	DB-IP-DC:PSX-CZ:TNF (30:69:1)	633	3 (30)	390 (100)	92^{int} (30)	18
4	7-DCST:DBDC:PATPD:ECZ:C_{60} (20:20:49.5:10:0.5)	633	2 (40)	112 (70)	$>90^{int}$ (40)	19
5	FDCST: PATPD-CAAN:ECZ (30:50:20)	532		200 (50)	$<90^{int}$ (>40)	20
6	H2:PVK:ECZ:C_{60} (25:49:25:1)	633	2.2 (41)	26 (44)	75^{int} (32)	21

[a] ext = external, int = internal.

Table 6. Our PR Composites and Their Measured Values for the Holographic Parameters[a]

PR composite 25:49:25:1 wt %	λ^{b}_{max},nm	α, cm^{-1}	η_{max}, % (E, V/μm)	Δn, $\times 10^{-3}$ (E, V/μm)	Γ^{c}, cm^{-1} (E, V/μm)
Dc:PVK:ECZ:C_{60}	401	$\sim$ 35	90 (56)	2.22 (63)	60 (63)
Ds:PVK:ECZ:C_{60}	382	$\sim$ 30	82 (63)	1.73 (63)	48 (59)

[a] A He−Ne laser (633 nm) was used. Sample thickness d = 110 μm; absorption coefficient α is for 633 nm. [b] Only for **Dc** and **Ds** in solution (chloroform). [c] For transmission geometry.

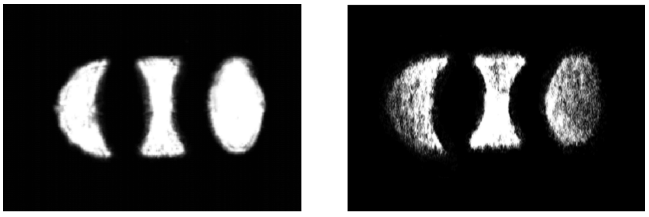

a) b)

Figure 7. (a) Photograph of CIO logo after transmission through the PR polymer. (b) Holographic image obtained through Bragg diffraction of the reading beam with **Dc**-based polymers at just an external applied electric field E = 20 V/μm.

A video in real time with this bidimensional hologram can be found in the Supporting Information. Phase stability of our samples is of several months and when there exist some damage, it is just enough to heat samples above 100 °C to recover their optical quality for some days more or even weeks.

4. CONCLUSIONS

We have fabricated high performance organic photorefractive composites functionalized with 25 wt % of our synthesized benzonitrile derivates nonlinear chromophores **Dc** and **Ds** with "push-pull" architecture and containing stilbazole-like backbone. NLO response for chromophores **Dc** and **Ds** evaluated by EFISH technique showed that the **Dc** chromophore has a larger $\mu\beta$ value than **Ds** due to non-planar conformation determined from X-ray diffraction analysis; the intramolecular hydrogen bond N···H−O promotes the planar conformation over **Dc**, these results are in good agreement with the theoretical prediction. For PR polymers based on the chromophore **Dc**, the diffraction efficiency peaks at just E = 56 V/μm with a value of 90% and for **Ds**, a maximum diffraction efficiency of 82% at E = 63 V/μm was observed. These are quite encouraging results since they were obtained for PR composites with performance at relatively low electric field (<60 V/μm) and with one of the lowest chromophore concentrations reported. Furthermore, these two chromophores have an excellent optical transparency in the visible region and due to the CN acceptor group on the main π-backbone instead of the NO_2 fragment as in DANS, H1 and H2; their compatibility with the polymer matrix could permit to increase concentration in PR devices to decrease the external applied electric field to continue having high diffraction efficiency and with an acceptable shelf-life time. The more bent conformation of **Ds** compound could partially explain the slightly better PR performance for polymers based on **Dc** than for those based on **Ds**, this fact might also be correlated with the theoretical and experimental $\mu\beta$ product. To demonstrate their dynamic holographic performance, a hologram of a two-dimensional object was recorded with a He−Ne laser at an applied electric field of only 20 V/μm.

■ ASSOCIATED CONTENT

Supporting Information. XRD profiles for **Dc** and **Ds** chromophores (CCDC Reference nos. 830814 and 830815), and a video in real time with a bidimensional hologram are available free of charge via the Internet at http://pubs.acs.org.

■ AUTHOR INFORMATION

Corresponding Author

*Phone: +52 (477) 441 4200; Fax: +52 (477) 441 4209; E. mail: jlmr@cio.mx.

■ ACKNOWLEDGMENT

This work was supported by CONACyT projects 55250, 49512, 58783, and, 83519 and UNAM PAPIIT IN-203207. Authors also thank M. Olmos for his technical assistance, M.A. Leyva for X-ray diffraction and CALMIP (Calcul en Midi Pyrénées-Toulouse, France) for computing facilities. Thanks are given to ICyT DF for a scholarship to E. N. Magaña-Vergara. Special thanks to Dr. B.A. Frontana-Uribe from CCIQS UAEMéx-UNAM for cyclic voltammetry measurements and fruitful discussions.

■ REFERENCES

(1) Ostroverkhova,O.Organic and Polymeric Photorefractive Materials and Devices . In *Introduction to Organic Electronic and Optoelectronic Materials and Devices*;Sun, S.-S., Dalton, L. R., Eds.; Taylor and Francis Group: Florida, USA, 2008, 607−636.

(2) Günter, P. Ed. *Nonlinear Optical Effects and Materials*; Springer-Verlag: Berlin, Germany, 2000.

(3) Günter, P., Huignard, J.-P., Eds. *Photorefractive Materials and Their Applications 2*; Springer: New York, USA, 2007.

(4) Thomas, J.; Norwood, R. A.; Peyghambarian, N. J. *Mater. Chem.* **2009**, *19*, 7476–7489.

(5) Blanche, P.-A.; Bablumian, A.; Voorakaranam, R.; Christenson, C.; Lin, W.; Gu, T.; Flores, D.; Wang, P.; Hsieh, W.-Y.; Kathaperumal, M.; et al. *Nature* **2010**, *468*, 80–83.

(6) Thomas, J.; Christenson, C. W.; Blanche, P.-A.; Yamamoto, M.; Norwood, R. A.; Peyghambarian, N. *Chem. Mater.* **2011**, *23*, 416–429.

(7) Ducharme, S.; Scott, J. C.; Tweig, R. J.; Moerner, W. E. *Phys. Rev. Lett.* **1991**, *66*, 1846–1849.

(8) Meerholz, K.; Volodin, B. L.; Sandalphon; Kippelen, B.; Peyghambarian, N. *Nature* **1994**, *371*, 497–500.

(9) Oh, J.-W.; Lee, C.; Kim, N. *J. Chem. Phys.* **2009**, *130* (134909), 1–6.

(10) Kukhtarev, N. V.; Markov, V. B.; Odulov, S. G.; Soskin, M. S.; Vinetskii, V. L. *Ferroelectrics* **1979**, *22*, 949–960.

(11) Nalwa, H. S., Miyata, S., Eds. *An Introduction to Photorefractive Polymers*; Kippelen, B.; Meerholz, K.; Peyghambarian, N. In *Nonlinear Optics of Organic Molecules and Polymers*; CRC Press Inc.: Boca Raton, USA, 1997, 465−513.

(12) Ostroverkhova, O.; Moerner, W. E. *Chem. Rev.* **2004**, *104*, 3267–3314.

(13) Maldonado, J. L.; Bishop, M.; Fuentes-Hernández, C.; Caron, P.; Domercq, B.; Barlow, S.; Thayumanavan, S.; Malagoli, M.; Manoharan, M.; Brédas, J.-L.; et al. *Chem. Mater.* **2003**, *15*, 994–999.

(14) Maldonado, J. L.; Ramos-Ortíz, G.; Meneses-Nava, M. A.; Barbosa-García, O.; Olmos-López, M.; Arias, E.; Moggio, I. *Opt. Mater.* **2007**, *29*, 821–826.

(15) Zhao, Z.; Li, Z.; Lam, J. W. Y.; Maldonado, J. L.; Ramos-Ortíz, G.; Liu, Y.; Yuan, W.; Xu, J.; Miao, Q.; Tang, B. Z. *Chem. Commun.* **2011**, *47*, 6924–6926.

(16) Kippelen, B.; Marder, S. R.; Hendrickx, E.; Maldonado, J. L.; Guillement, G.; Volodin, B. L.; Steele, D. D.; Enami, Y.; Sandalphon; Yao, Y. J.; et al. *Science* **1998**, *279*, 54–57.

(17) Hendrickx, E.; Herlocker, J.; Maldonado, J. L.; Marder, S. R.; Kippelen, B.; Persoons, A.; Peyghambarian, N. *Appl. Phys. Lett.* **1998**, *72*, 1679–1681.

(18) Joo, W.-J.; Kim, N.-J.; Chun, H.; Moon, I. K.; Kim, N. *Polymer* **2001**, *42*, 9863–9866.

(19) Thomas, J.; Fuentes-Hernández, C.; Yamamoto, M.; Cammack, K.; Matsumoto, K.; Walker, G. A.; Barlow, S.; Kippelen, B.; Meredith, G.; Marder, S. R.; et al. *Adv. Mater.* **2004**, *16*, 2032–2036.

(20) Tay, S.; Blanche, P.-A.; Voorakaranam, R.; Tunc, A. V.; Lin, W.; Rokutanda, S.; Gu, T.; Flores, D.; Wang, P.; Li, G.; et al. *Nature* **2008**, *451*, 694–698.

(21) Maldonado, J. L.; Ponce-de-León, Y.; Ramos-Ortíz, G.; Rodríguez, M.; Barbosa-García, O.; Meneses-Nava, M. A.; Santillan, R.; Farfán, N. *J. Phys. D Appl. Phys.* **2009**, *42* (075102), 1–6.

(22) Wurthner, F.; Wortmann, R.; Meerholz, K. *ChemPhysChem* **2002**, *3*, 17–31.

(23) Marder, S. R.; Kippelen, B.; Jen, A. K.; Peyghambarian, N. *Nature (London)* **1997**, *388*, 845–851.

(24) Moon, K.; Kim, N. *Dyes Pigm.* **2009**, *82*, 322–328.

(25) Li, H.; Termine, R.; Angiolini, L.; Giorgini, L.; Mauriello, F.; Golemme, A. *Chem. Mater.* **2009**, *21*, 2403–2409.

(26) Oh, J.-W.; Joo, W.-J.; Moon, I. K.; Choi, C.-S.; Kim, N. *J. Phys. Chem. B* **2009**, *113*, 1592–1597.

(27) Cheng, L. T.; Tam, W.; Marder, S. R.; Stiegman, A. E.; Rikken, G.; Spangler, C. W. *J. Phys. Chem.* **1991**, *95*, 10643–10652.

(28) Zilker, S. J. *ChemPhysChem* **2000**, *1*, 72–87.

(29) Volodin, B. L.; Sandalphon; Meerholz, K.; Kippelen, B.; Kukhtarev, N. V.; Peyghambarian, N. *Opt. Eng.* **1995**, *34*, 2213–2223.

(30) Angelone, R.; Ciardelli, F.; Colligiani, A.; Greco, F.; Masi, P.; Romano, A.; Ruggeri, G. *ChemPhysChem* **2010**, *11*, 460–465.

(31) Rodríguez, M.; Maldonado, J. L.; Ramos-Ortíz, G.; Lamère, J. F.; Lacroix, P. G.; Farfán, N.; Ochoa, M. E.; Santillan, R.; Meneses-Nava, M. A.; Barbosa-García, O.; et al. *New J. Chem.* **2009**, *33*, 1693–1702.

(32) Lacroix, P. G.; Averseng, F.; Malfant, I.; Nakatani, K. *Inorg. Chim. Acta* **2004**, *357*, 3825–3835.

(33) Meyer, C. D.; Joiner, C. S.; Stoddart, J. F. *Chem. Soc. Rev.* **2007**, *36*, 1705–1723.

(34) Sheldrick, G. M. SHEXL-97. *Program For Crystal Structure Solution*; University of Göttingen: Germany, 1997.

(35) Levine, B. F.; Betha, C. G. *J. Chem. Phys.* **1975**, *63*, 2666–2682.

(36) Accelrys Software Inc., Materials Studio Release Notes, Release 5.5, San Diego: Accelrys Software Inc., 2010.

(37) Zerner, M. C.; Loew, G. H.; Kirchner, R. F.; Mueller-Westerhoff, U. T. *J. Am. Chem. Soc.* **1980**, *102*, 589–599.

(38) Choudhury, K. R.; Samoc, M.; Patra, A.; Prasad, P. N. *J. Phys. Chem. B* **2004**, *108*, 1556–1562.

(39) Maldonado, J. L.; Ramos-Ortíz, G.; Barbosa-García, O.; Meneses-Nava, M. A.; Márquez, L.; Olmos-López, M.; Reyes, H.; Muñoz, B. M.; Farfán, N. *Int. J. Mod. Phys. B* **2007**, *21*, 2625–2634.

(40) Kwon, O.-P.; Montemezzani, G.; Günter, P.; Lee, S.-H. *Appl. Phys. Lett.* **2004**, *84*, 43–45.

(41) Eralp, M.; Thomas, J.; Tay, S.; Blanche, P.-A.; Schülzgen, A.; Norwood, R. A.; Yamamoto, M.; Peyghambarian, N. *Opt. Express* **2007**, *15*, 11622–11628.

(42) Gallego-Gomez, F.; Salvador, M.; Köber, S.; Meerholz, K. *Appl. Phys. Lett.* **2007**, *90* (251113), 1–3.

(43) Fuentes-Hernández, C.; Suh, D. J.; Kippelen, B.; Marder, S. *Appl. Phys. Lett.* **2004**, *85*, 534–536.

(44) Domínguez, O.; Rodríguez-Molina, B.; Rodríguez, M.; Ariza, A.; Farfán, N.; Santillan, R. *New J. Chem.* **2011**, *35*, 156–164.

(45) Lesly, T. M.; Martino, R. N.; Choe, E. W.; Khanarian, G.; Hass, D.; Nelson, G.; Stamatoff, J. B.; Stuetz, D. E.; Teng., C. C.; Yoon, Y. N. *Mol. Cryst. Liq. Cryst.* **1987**, *153*, 451–477.

(46) Kumaresan, D.; Thummel, R. P.; Bura, T.; Ulrich, G.; Ziessel, R. *Chem.—Eur. J.* **2009**, *15*, 6335–6339.

(47) William, D. J. *Angew. Chem., Int. Ed. Engl.* **1984**, *23*, 690–703.

(48) Oudar, J. L. J. *Chem. Phys.* **1977**, *67*, 446–457.

(49) Oudar, J. L.; Chemla, J. *J. Chem. Phys.* **1977**, *66*, 2664–2668.

(50) Hendrickx, E.; Wang, J. F.; Maldonado, J. L.; Volodin, B. L.; Sandalphon; Mash, E. A.; Kippelen, B.; Peyghambarian, N. *Macromolecules* **1998**, *31*, 734–739.

(51) Ding, L.; Jiang, D.; Huang, J.; Erdan, G.; Liu, L.; Chai, Z.; Liu, D. *J. Phys. Chem. C* **2008**, *112*, 10266–10272.

(52) Winiarz, J. G. *J. Phys. Chem. C* **2007**, *111*, 1904–1911.

(53) Tay, S.; Thomas, J.; Eralp, M.; Li, G.; Kippelen, B.; Marder, S. R.; Meredith, G.; Schülzeng, A.; Peyghambarian, N. *Appl. Phys. Lett.* **2004**, *85*, 4561–4563.

(54) Kogelnik, H. *Bell Syst. Tech. J.* **1969**, *48*, 2909–2947.